Available online at www.sciencedirect.com
SCIENCE DIRECT®
International Journal of Thermal Sciences 44 (2005) 610–622
International Journal of Thermal Sciences
www.elsevier.com/locate/ijts

Models for droplet transient heating: Effects on droplet evaporation, ignition, and break-up

S.S. Sazhin *, W.A. Abdelghaffar, E.M. Sazhina, M.R. Heikal

School of Engineering, Faculty of Science and Engineering, University of Brighton, Cockcroft Building, Brighton BN2 4GJ, UK

Received 5 November 2004; received in revised form 7 February 2005; accepted 7 February 2005

Available online 8 April 2005

Abstract

The effect of the temperature gradient inside fuel droplets on droplet evaporation, break-up and the ignition of fuel vapour/air mixture is investigated based on a zero-dimensional code. This code takes into account the coupling between the liquid and gas phases and describes the autoignition process based on the eight step chain branching reaction scheme (the Shell model). The effect of temperature gradient inside droplets is investigated by comparing the 'effective thermal conductivity' model and the 'infinite thermal conductivity' model, both of which have been implemented in the zero-dimensional code. The predictions of the code are validated against available experimental data. It is pointed out that in the absence of break-up, the influence of the temperature gradient in droplets on droplet evaporation in a realistic diesel engine environment is generally small (a few percent). In the presence of the break-up process, however, the temperature gradient inside the droplets can lead to a significant decrease in evaporation time. This is attributed to the fact that the effect of temperature gradient inside droplets leads to a substantial increase in droplet surface temperature at the initial stages of its heating. This is translated into a decrease in surface tension and the threshold radii of the unstable droplets. Even in the absence of break-up, the effect of the temperature gradient inside the droplets leads to a noticeable decrease in the total ignition delay. In the presence of break-up this effect is enhanced substantially, leading to more than halving of the total ignition delay. It is recommended that the effect of the temperature gradient inside the droplets is taken into account in computational fluid dynamics codes describing droplet break-up and evaporation processes, and the ignition of the evaporated fuel/air mixture.

Keywords: Droplet heating; Conduction; Radiation; Evaporation; Diesel fuel; Ignition; Break-up

1. Introduction

The problem of droplet heating by convection and radiation have been widely discussed in the literature [1–10]. However, the models widely used in most practical engineering applications tend to be rather simple. This is due to the fact that droplet heating and evaporation have to be modelled alongside the effects of turbulence, combustion, droplet break-up and related phenomena in realistic 3D enclosures. Hence, finding a compromise between the complexity of the models and their computational efficiency is the essential precondition for successful modelling. In a series of papers [11–19] an attempt was made to develop simplified models for droplet heating; sophisticated underlying physics was described using relatively simple mathematical tools. Some of these models, including those taking into account the effects of temperature gradient inside droplets, recirculation inside them and their radiative heating, were implemented into numerical codes focused on simulating droplet heating [20,21]. In [20] the effect of recirculation was taken into account using the so-called 'effective thermal conductivity model' [5], where this effect was approximated by replacing the actual liquid thermal conductivity by the effective thermal conductivity (depending on the droplet's Peclet number). The effect of finite thermal conductivity of droplets was taken into ac-

* Corresponding author.
E-mail address: s.sazhin@brighton.ac.uk (S.S. Sazhin).

1290-0729/$ – see front matter
doi:10.1016/j.ijthermalsci.2005.02.004

Nomenclature

a	coefficient introduced in Eq. (6)	m^{-b}
A	cross-sectional area	m^2
A_{f4}	coefficient in the Shell model	
b	coefficient introduced in Eq. (6)	
B	Spalding number	
c	specific heat capacity	$J{\cdot}kg^{-1}{\cdot}K^{-1}$
C_D	drag coefficients	
D	binary diffusion coefficient	$m^2{\cdot}s^{-1}$
f	function introduced in Eq. (2)	
F	function introduced in Eq. (3)	
k	thermal conductivity	$W{\cdot}m^{-1}{\cdot}K^{-1}$
L	specific heat of evaporation	$J{\cdot}kg^{-1}$
Nu	Nusselt number	
Q_a	efficiency factor of absorption	
Q_L	power spent on droplet heating	W
p	pressure	Pa
Pr	Prandtl number	
R	radius	m
Re	Reynolds number	
Sc	Schmidt number	
Sh	Sherwood number	
t	time	s
T	temperature	K
$\mathbf{v}$	velocity vector	$m{\cdot}s^{-1}$
We	Weber number	

Greek symbols

α	coefficient introduced in Eq. (11)	
μ	dynamic viscosity	$N{\cdot}s{\cdot}m^{-2}$
ν	kinematic viscosity	$m^2{\cdot}s^{-1}$
ρ	density	$kg{\cdot}m^{-3}$
σ	surface tension	$N{\cdot}m^{-1}$

Subscripts

a	air
b	boiling or bag
cr	critical
d	droplet
eff	effective
ext	external
F	fuel vapour
fs	saturated fuel vapour
g	gas
M	mass
p	constant pressure
s	surface or stripping
T	temperature
0	initial or non-evaporating
∞	far from the droplet

Superscripts

$\bar{}$	average
$\tilde{}$	normalized

count based on the analytical solution of the heat conduction equation inside droplets under the assumption that the convection heat transfer coefficient does not change during the time step used in the numerical code. Two models of thermal radiation absorption in droplets were used. These were the model suggested in [14], describing the distributed radiation source and the simplified model, describing the integral absorption of thermal radiation, suggested in [11,15]. In the latter case the uniform distribution of the radiation source was assumed. The predictions of both models turned out to be very close which allowed the authors of [20] to recommend the application of the simplified model. In this model the efficiency factor of absorption was approximated as aR_d^b, where R_d is the droplet radius, a and b are polynomials of external temperature. It was shown that this code is more accurate and computer efficient when compared with the approach to numerical modelling of droplet heating based on the numerical solution of the heat conduction equation inside droplets [22].

In [21] the 'extended' and effective thermal conductivity models of droplet vaporization developed in [5] were generalized to take into account the contribution of thermal radiation and the temperature dependence of liquid fuel properties. In the 'extended' model the convection of liquid was explicitly taken into account. As in [20], in both models the contribution of thermal radiation was taken into account based on the model for thermal radiation absorption suggested in [14]. Comparison between the calculations performed using the 'extended' model and distributed radiation absorption heat source and those based on the effective thermal conductivity model with the uniform distribution of the internal heat source showed exceptionally good agreement between the results. This allowed the authors to recommend using the effective thermal conductivity model with uniform radiation absorption for modelling of droplet heating and evaporation. This conclusion is in agreement with the above-mentioned results reported in [20], which were focused on the effective thermal conductivity model only.

This paper is focused on further development of the model described in [20], its testing and application to modelling the processes of heating, evaporation, ignition and break-up of diesel fuel droplets. In contrast to the original paper [20], the effect of droplets' velocities, heating and evaporation on the surrounding gas is taken into account (coupled solutions). The surrounding gas will be accelerated by movement of the droplets. Then the gas will cool with accompanying heating and evaporation of droplets. The fuel vapour will diffuse through the gas culminating in ignition

of the fuel vapour/air mixture. These effects are expected to be accelerated significantly via droplet break-up [23]. The model is implemented into a zero-dimensional code in which all values of the gas parameters (velocity, temperature, fuel vapour concentration etc) are assumed to be homogeneous.

Naturally, while the main focus of this paper is on the effects produced by the temperature gradients in droplets, a number of important processes will be beyond its scope. These include the effects of real gases [24], near critical and supercritical droplet heating [25,26], analysis of droplets' collisions and coalescence [27,28].

The main equations and approximations used in this code are described in Section 2. In Section 3 this code is tested against several available experimental data. Results of sensitivity studies of the effects of temperature gradient inside droplets on droplet evaporation time, ignition delay and the break-up process are discussed in Section 4. The main results of the paper are summarised in Section 5.

2. Basic equations and approximation

A model for droplet heating, taking into account the temperature gradient inside it and the effect of thermal radiation, for fixed gas parameters have already been described in our previous paper [20]. The focus of this section will be on the new elements of the model, which take into account the effects of droplets on gas.

A number of correlations for the Nusselt number (Nu) of moving and evaporating droplets have been suggested. The one for non-evaporating droplets, which is most widely used is presented as [29]:

$$Nu_0 = 2 + 0.6\,Re_d^{1/2} Pr_d^{1/3} \tag{1}$$

where $Re_d = 2R_d|\mathbf{v}_d - \mathbf{v}_g|/\nu_g$ and $Pr_d = c_{pg}\mu_g/k_g$ are Reynolds and Prandtl numbers of the moving droplets, $\mathbf{v}_d$ and $\mathbf{v}_g$ are droplet and gas velocities, ν_g and μ_g are gas kinematic and dynamic viscosities, c_{pg} and k_g are gas specific heat capacity at constant pressure and thermal conductivity (the temperature dependence of these parameters is taken into account). Sometimes the coefficient 0.6 in Eq. (1) is replaced by 0.552 [5].

An alternative correlation for Nu_0 was suggested in the form [5]:

$$Nu_0 = 1 + (1 + Re_d Pr_d)^{1/3} f(Re_d) \tag{2}$$

where

$$f(Re_d) = \begin{cases} 1 & \text{when } Re_d \leqslant 1 \\ Re_d^{0.077} & \text{when } 1 < Re_d \leqslant 400 \end{cases}$$

Correlation (2) is believed to be more accurate than (1) at $Re_d < 10$ [5]. However, the difference between the predictions of these correlations for $0 < Re_d \leqslant 400$ does not exceed about 10%. This is well within the margins of errors of experimental measurements of parameters used in these equations. Our analysis will be based on Eq. (1)—the simpler one.

The effect of finite film thickness, and evaporation and heating of fuel vapour can be accounted for by modifying Nu_0 to [5,9]:

$$Nu = \frac{2\ln(1+B_T)}{B_T}\left[1 + 0.3\frac{Re_d^{1/2} Pr_d^{1/3}}{F(B_T)}\right] \tag{3}$$

where

$$F(B_T) = (1+B_T)^{0.7}\frac{\ln(1+B_T)}{B_T}$$

$$B_T = \frac{c_{pF}(T_g - T_s)}{L_{\text{eff}}}$$

is the Spalding temperature number, $L_{\text{eff}} = L + \frac{Q_L}{\dot{m}}$, Q_L is the power spent on droplet heating, c_{pF} is the specific heat capacity of fuel vapour, T_g and T_s are ambient gas temperature, and droplet surface temperature respectively, L is the specific latent heat of evaporation.

Note some printing mistakes on pages 37 and 38 of [9]: c_p should be replaced by c_{pF} in Eq. (2.56b); $Sc^{1/3}$ and $Pr^{1/3}$ are missing in the numerator and denominator respectively of Eq. (2.57); $k/2$ should be removed from the last formula on page 37 and the second formula on page 38.

Following widely used practice (see, e.g., [2,4]) a simplified version of Eq. (3) will be used in our analysis:

$$Nu = \frac{2\ln(1+B_M)}{B_M}\left[1 + 0.3\,Re_d^{1/2} Pr_d^{1/3}\right] \tag{4}$$

where B_M is the Spalding mass number [5] (for the details of its calculations see [16]). This is justified by the fact that the focus of the paper is on the investigation of the effect of temperature gradient inside droplets on evaporation, break-up and ignition processes, and not on the most accurate modelling of these processes. The corrections introduced by Eq. (3) are not expected to influence the conclusions of this paper. Moreover they can, on some occasions, even marginally decrease the accuracy of calculations of the mass flow rate of evaporated fuel [30]. Heat removed from the gas is described by Eq. (1). Gas temperature was calculated from the equation:

$$\frac{dT_g}{dt} = -2\pi\frac{k_g}{m_g c_{pg}}\sum_i Nu_{0i} R_{di}(T_g - T_{si}) \tag{5}$$

where m_g is the total mass of gas, T_{si} are droplets' surface temperatures, subscripts i indicate individual droplets, and summation is performed over all droplets. Gas mass and droplets' radii are updated at each time step to take into account droplet evaporation.

Effects of recirculation inside droplets and the temperature gradient in them are taken into account as in [20]. It is assumed that thermal radiation is absorbed in droplets homogeneously with the average absorption efficiency factor defined as:

$$\overline{Q}_a = a R_d^b \tag{6}$$

where a and b are polynomials of the external temperature T_{ext} [15].

As mentioned in Introduction, more complex models which take into account the differential absorption of thermal radiation in droplets [14] give only minor improvements in the accuracy of prediction of $\overline{Q}_a$ [20,21]. These can be safely ignored in most practical applications.

The mass vaporization rate from the droplet surface is described by the following equation [5]:

$$\dot{m}_d = 2\pi \bar{\rho}_g \overline{D}_g R_d Sh_0 \ln(1 + B_M) \tag{7}$$

where $\bar{\rho}_g$ and $\overline{D}_g$ are average gas density and binary diffusion coefficient, Sh_0 is the Sherwood number of non-evaporating droplets, approximated as [29]:

$$Sh_0 \equiv 2h_m R_d/\overline{D}_g = 2 + 0.6 Re_d^{1/2} Sc_d^{1/3} \tag{8}$$

h_m is the mass transfer coefficient, $Sc_d = \nu/\overline{D}_g$ is the Schmidt number. As in the case of heat transfer, approximation (8) gives the results close to those predicted by other approximations [5,9]. The effect of thermal film thickness is considered to be small [30]. Droplet swelling due to thermal expansion was taken into account. Kinetic effects on droplet evaporation are ignored [16].

The droplet dynamics is described by the following equation [5]:

$$m_d \frac{\mathrm{d}\mathbf{v}_d}{\mathrm{d}t} = -\frac{C_{D0}}{2} \bar{\rho}_g (\mathbf{v}_d - \mathbf{v}_g)|\mathbf{v}_d - \mathbf{v}_g| A_d \tag{9}$$

where $A_d = \pi R_d^2$ is the cross-sectional area of droplets, C_{D0} is the drag coefficient for non-evaporating droplets, depending on Re_d. A number of approximations for C_{D0} have been suggested [33,34]. Our analysis will be based on the following approximation [35]:

$$C_{D0} = \begin{cases} \frac{24}{Re_d}\left(1 + \frac{1}{6} Re_d^{2/3}\right) & \text{when } Re_d \leqslant 1000 \\ 0.424 & \text{when } Re_d > 1000 \end{cases} \tag{10}$$

The effect of evaporation is taken into account via replacing C_{D0} by [5]:

$$C_D = -\frac{C_{D0}}{(1 + B_M)^{\alpha}} \tag{11}$$

where

$$\alpha = \begin{cases} 1 & \text{when } B_M < 0.78 \\ 0.75 & \text{when } B_M \geqslant 0.78 \end{cases}$$

The momentum transferred from gas to droplets has the same value but the opposite sign to the momentum transferred from droplets to gas. Gas velocity is calculated from the momentum conservation equation, which can be presented in the form:

$$\frac{\mathrm{d}(m_g \mathbf{v}_g)}{\mathrm{d}t} = -\sum_i \frac{\mathrm{d}(m_{di} \mathbf{v}_{di})}{\mathrm{d}t} \tag{12}$$

Two types of stresses acting on the moving droplets are taken into account. These are normal stresses, leading to droplet 'bag' break-up, and tangential stresses, leading to droplet 'stripping' break-up [23]. In both cases, the reduction of droplet radii is described by the equation:

$$\frac{\mathrm{d}R_d}{\mathrm{d}t} = \begin{cases} 0 & \text{when } R_d \leqslant R_{db(s)} \\ -\frac{(R_d - R_{db(s)})}{t_{b(s)}} & \text{when } R_d > R_{db(s)} \end{cases} \tag{13}$$

where $R_{db(s)}$ are threshold radii of marginally stable droplets with respect to bag (stripping) break-ups, $t_{b(s)}$ are the characteristic times of the development of these break-ups [23]:

$$R_{db} = \frac{6\sigma_s}{\bar{\rho}_g |\mathbf{v}_g - \mathbf{v}_d|^2}, \qquad R_{ds} = \frac{0.5\sigma_s^2}{\bar{\rho}_g^2 |\mathbf{v}_g - \mathbf{v}_d|^3 \nu_g},$$

$$t_b = \pi \left[\frac{\rho_d R_d^3}{2\sigma_s}\right]^{1/2}, \qquad t_s = \frac{13 R_d}{|\mathbf{v}_g - \mathbf{v}_d|} \sqrt{\frac{\rho_d}{\bar{\rho}_g}}$$

σ_s is the surface tension coefficient, $\bar{\rho}_g$ is the average gas density, calculated as the average mass density of the ambient air ρ_a and the average fuel vapour density $\bar{\rho}_{Fv}$. The latter is calculated as

$$\bar{\rho}_{Fv} = (\rho_{F\infty} + 2\rho_{Fs})/3 \tag{14}$$

$\rho_{F\infty}$ is the ambient fuel vapour density, ρ_{Fs} is the saturated fuel vapour density near the droplet surface.

The threshold values R_{db} and R_{ds} follow from the criteria for bag and stripping break-ups given in [36,37]:

$$We \equiv \frac{\bar{\rho}_g |\mathbf{v}_g - \mathbf{v}_d|^2 R_d}{\sigma} > 6$$

(bag break-up), and

$$\frac{We}{\sqrt{Re}} > 0.5$$

(stripping break-up), where We is the Weber number.

The contribution from catastrophic break-up has been ignored. This is likely to occur at rather large We (greater than about 350 [31,32]), and is not expected to be observed for small droplets in diesel engines away from the immediate vicinity of the nozzle. An alternative equation for the evolution of droplet mass during the development of break-up has been discussed in [32] (see his Eq. (3)). A detailed analysis of the latter equation and its comparison with our Eq. (13) is beyond the scope of this paper.

The gradients of temperature and fuel vapour concentration in the gas phase are ignored. This has been introduced with a view to the future implementation of the algorithm into a computational fluid dynamics (CFD) code, where this assumption refers to individual computational cells. The number of droplets in the enclosure can be arbitrary, but the direct interaction between droplets is not taken into account at this stage. All transport coefficients for the gas phase were calculated at average temperatures defined as [4]:

$$\overline{T} = (T_g + 2T_s)/3 \tag{15}$$

The concentration of fuel vapour is assumed to be so small that its effect on transport coefficients can be ignored. This

effect could be taken into account as described in Appendix 3 of [38]. It was taken into account when calculating gas density (as described above) and average specific heat capacity (following the same procedure as for the average gas density).

The ignition of the fuel vapour/air mixture is described based on the Shell autoignition model in which the autoignition process is reduced to the eight-step chain branching reaction scheme [39]. We used the version of this model developed in [40,41] with A_{f4} in the range between 3×10^6 and 6×10^6.

3. Validation of the numerical algorithm

The only direct observations of temperature gradient inside large ($R_d > 100$ μm) droplets are those reported in [42–44], to the best of our knowledge. This is not directly relevant to diesel engine environment as droplets are typically much smaller there. Also, the results reported by these authors refer to instantaneous measurements and cannot be used for validating the model for droplet heating process described above. In this section we will validate our model by comparing the predicted time evolution of droplet radius and the predicted ignition delay with experimental observations. This seems to be the only feasible approach.

In the experiment conducted by Belardini et al. [45], 10^{-9} g of tetradecane was injected at a temperature of 300 K and initial velocity of 6 m·s^{-1} through a hole of 0.28 mm diameter into a 100 cm^3 chamber. The chamber was filled with air at 1 bar, and the initial temperatures were in the range from 473 to 673 K. The evolution of droplet diameter during the evaporation process was measured starting with droplet diameter equal to 72 μm. The results of measurements were presented in the form of a plot of $(R_d/R_{d0})^2$ versus time t and are shown in Fig. 1. In the same figure, the time evolution of this variable, predicted by the algorithm described in Section 2, is presented. The calculations were performed using the effective thermal conductivity model (hereafter referred to as ETC model), and infinite thermal conductivity model (hereafter referred to as ITC model). The physical properties of tetradecane, used in the calculations, are given in Appendix A.

As follows from Fig. 1, the results of calculations for both ITC and ETC models show reasonable agreement with the measurements for both temperatures 473 and 673 K. In fact the predictions of the ETC and ITC models are practically indistinguishable. This difference would have been observed for the surface temperatures at the initial stage of heating, but this is not translated into the time evolution of droplet radius. The plots of $(R_d/R_{d0})^2$ versus t are non-linear functions of time after the completion of the heat-up period, in contrast to the prediction of the d^2-law (this is particularly clearly seen for the curve referring to $T_s = 673$ K). This is attributed to the effect of thermal radiation which was not taken into account when deriving this law (cf. the following discussion

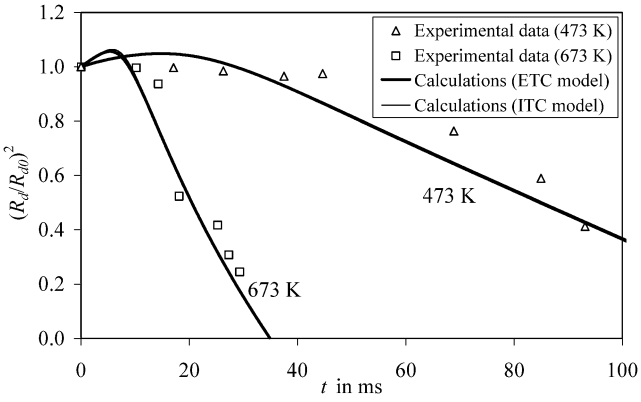

Fig. 1. The values of $(R_d/R_{d0})^2$ for evaporating tetradecane droplets versus time, as measured by Belardini et al. [45], and the results of calculations based on the ITC (infinite thermal conductivity) and the ETC (effective thermal conductivity) models implemented into the algorithm described in Section 2. The ETC model takes into account the effect of temperature gradient in droplets, while the ITC model does not take it into account. The values of the initial gas temperatures 473 and 673 K are indicated near the plots.

referring to Fig. 3). The effect of thermal radiation generally decreases with decreasing droplet radius [15].

Data for $T_{g0} = 673$ K presented in Fig. 1 was used in [22] to validate various models for droplet heating. The comparison was between: a model which includes the effect of finite thermal conductivity inside droplets (but not recirculation) combined with the effect of droplet swelling; and a model which did not take into account the effect of swelling. As expected, the prediction of the first model was practically indistinguishable from that shown in Fig. 1. Ignoring the effect of swelling, however, led to visibly poorer agreement between experimental data and the prediction of the model.

The experimental data reported in [46] were obtained for a suspended n-heptane droplets in nitrogen atmosphere at pressures in the range between 0.1 and 1 MPa and temperatures in the range between 400 and 800 K. Droplet initial radii varied from 0.3 to 0.35 mm. The experiments were performed under microgravity conditions. The experimentally observed values of $(R_d/R_{d0})^2$ versus t for pressure 0.1 MPa, initial gas temperatures 471, 555, 648, 741 K, and the initial droplet radii equal to 0.3 mm, are shown in Fig. 2. Also, the results of calculations based on ETC and ITM models for the same values of parameters are shown. The physical properties of n-heptane used in calculations are given in Appendix A.

As follows from Fig. 2, both ITC and ETC models show good agreement with experimental data. For $T_{g0} = 471$ K and $T_{g0} = 555$ K the predictions of the models practically coincide. At higher temperatures, however, the predictions of the ETC model are in marginally better agreement with experimental data, compared with the ITC model, as expected. At lower initial gas temperatures, droplets evaporate more slowly and the temperature inside droplets has sufficient time to become almost homogeneous. Hence, the closeness of evaporation times predicted by the ETC and ITC models. Stronger effect of droplet finite thermal conduc-

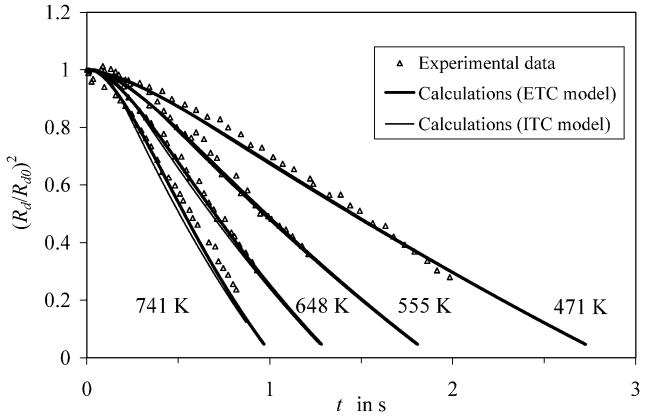

Fig. 2. The values of $(R_d/R_{d0})^2$ for evaporating n-heptane droplets versus time for the initial pressure of 0.1 MPa, as measured by Nomura et al. [46], and the results of calculations based on the ITC and the ETC models implemented into the algorithm described in Section 2. The values of the initial gas temperatures 471, 555, 647 and 741 K are indicated near the plots.

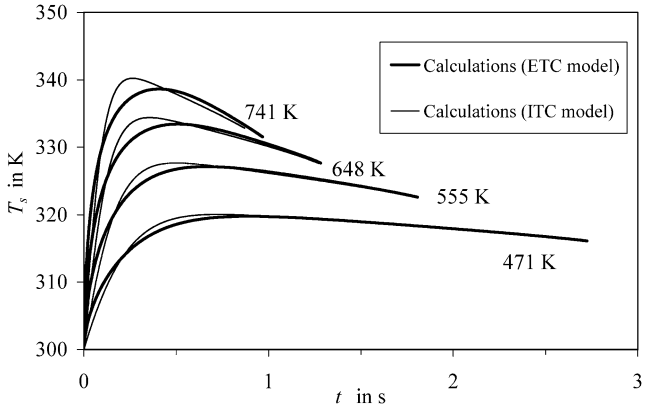

Fig. 3. The plots of T_s versus time for the same values of parameters as in Fig. 2, calculated using the ITC and the ETC models implemented into the algorithm described in Section 2.

tivity on the evolution of their size shown in Fig. 2, compared with Fig. 1, is related to much larger droplets studied in [46] compared with [45].

Plots of droplets surface temperatures T_s versus t for the same parameters as in Fig. 2 are shown in Fig. 3. As follows from this figure, the ETC model predicts much quicker rise of surface temperature compared with the ITC model at the initial stage. This is related to the fact that the heat reaching the surface of the droplet is spent on heating the whole droplet in the ITC model, and on the heating of a relatively thin layer near the droplet surface in the ETC model. Then the surface temperature predicted by the ETC model becomes lower than the one predicted by the ITC model. This is related to the fact that the increased surface temperature predicted by the ETC model will lead to a decrease in the amount of heat supplied to the droplet. Eventually, the surface temperatures predicted by both models become practically indistinguishable, as in the case considered earlier. Note that both ITC and ETC models predict the maximal values of droplet surface temperature at certain moments of

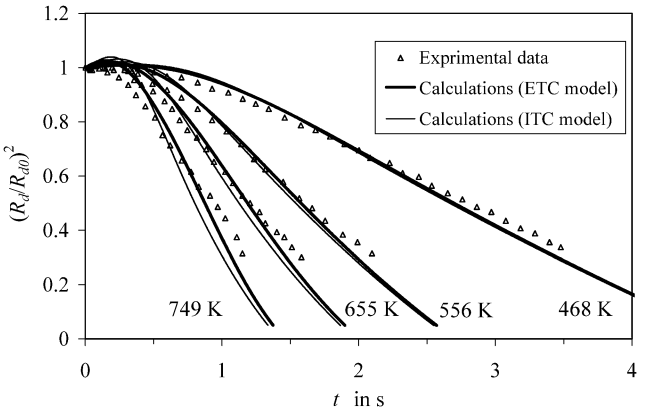

Fig. 4. The same as in Fig. 2 but for the initial gas pressure of 0.5 MPa.

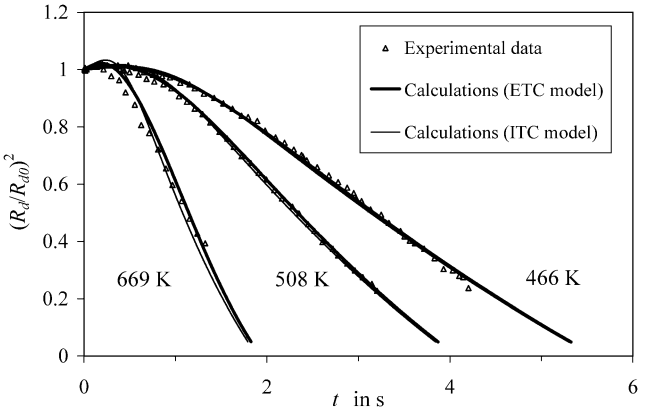

Fig. 5. The same as in Fig. 2 but for the initial gas pressure of 1 MPa.

time. These maxima are related to the contribution of thermal radiation. This result agrees with that reported in [21]. The detailed physical explanation of this phenomenon is given in [21]. In the absence of radiation the droplet surface temperature is expected to increase asymptotically to the wet bulb temperature. Note that temperatures shown in this figure are well below the n-heptane boiling temperature 371.4 K.

The plots similar to those shown in Fig. 2 but for pressures 0.5 MPa and 1 MPa, and various initial gas temperatures are shown in Figs. 4 and 5. As follows from these figures, the ETC model predicts marginally more accurate results compared with the ITC one, similarly to the case of lower pressure (see Fig. 2). The corresponding plots of T_s versus t have the properties similar to those shown in Fig. 3 for pressure 0.1 MPa.

The experimental data discussed so far is relevant to understanding heating and evaporation processes—it does not give us much information about the influence of droplets on gas. In what follows, we compare experimental data on the total ignition delay times reported in [47] and the prediction of the models. In the experiment described in this paper, n-heptane droplets with the initial radii of 0.35 mm were suspended in air at pressure 0.5 MPa. The droplets' diameters were measured within ± 0.05 mm. A furnace able to gener-

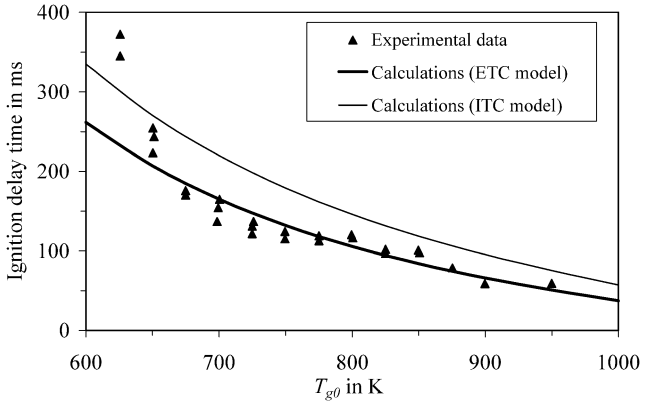

Fig. 6. The values of the total ignition delay time for evaporating n-heptane droplets versus initial gas temperature, as measured by Tanabe et al. [47], and the results of calculations based on the ITC and the ETC models implemented into the algorithm described in Section 2. The version of the Shell autoignition model described in [40,41] was used with the coefficient $A_{f4} = 3 \times 10^6$. The ratio of the volumes of air and liquid droplet was taken equal to $19.1^3 = 6967.871$ to provide the equivalence ratio 0.5 for $T_{g0} = 600$ K.

ate almost uniform gas temperature (from room temperature to 1100 K) was constructed and used for this experiment. The igniting droplets were observed by a Michelson interferometer so that the time dependent temperature distribution around the droplets could be estimated. Interferometric images were stored on an 8 mm video tape with a frame rate of 50 s^{-1} and were analysed by computer image processing. The experiment was performed under microgravity conditions by using a 110 m drop tower. This enabled the authors to observe spherically symmetrical phenomenon, that could be compared with the one-dimensional theoretical analysis [47].

The volume of air used in the experiment was not specified, but it can be assumed that this volume was rather large. Hence, we took lean ignition limit when the equivalence ratio equal to 0.5 for the initial gas temperature $T_{g0} = 600$ K [41]. This corresponds to the case when the radius of air is equal to 19.1 radii of droplets. This volume could be identified with the so-called 'cooling zone' [48,49]. The observed total ignition delay times (physical + chemical ignition delays) versus initial gas temperatures are shown in Fig. 6. In the same figure the total ignition delay times predicted by the ETC and ITC models are shown. The calculations were based on the Shell model with $A_{f4} = 3 \times 10^6$.

As follows from Fig. 6, the influence of the temperature gradient in droplets on the total ignition delay is noticeably greater than its influence on droplet evaporation time discussed earlier. This is related to the fact that the chemical part of the total ignition delay is a strongly non-linear function of gas temperature in the vicinity of droplets determined by Eq. (15). As shown earlier (see Fig. 3), the droplet surface temperature strongly depends on the temperature gradient in droplets, especially at the initial stages of heating. Hence, this temperature gradient cannot be ignored when calculating the total ignition delay of fuel droplets. If the ETC model is replaced by the ITC model for the same set of parameters then the agreement between the predicted and observed total ignition delays become much worse for $T_{g0} > 650$ K (see Fig. 6). This shows that the effects of temperature gradient inside droplets influence significantly the total ignition delay and need to be taken into account when modelling this phenomenon. The rapid increase of the ignition delay with decrease of T_{g0} in the range 600–650 K is not reproduced well by either model. This could be related to the fact that both models do not take into account the heat losses from the combustion chamber. In the case of short total ignition delays at large initial gas temperatures, these effects of heat loss can be ignored, but they need to be taken into account in the case of relatively long total ignition delays at low gas temperatures (cf. the results reported in [40]). The analysis of this effect is beyond the scope of this paper.

4. Application to a monodisperse spray

This section will focus on the investigation of the effects of temperature gradient inside droplets and recirculation in them on droplet velocity, break-up, heating and evaporation, and the ignition of fuel vapour/air mixture in a monodisperse spray. The algorithm described in Section 2, and validated in Section 3 will be used. The fuel was approximated by n-dodecane, and the 'average' diesel fuel, the characteristics of which were takes from various sources (see Appendix A).

The overall volume of injected liquid fuel was taken equal to 1 mm^3, and the volume of air where the fuel was injected was taken equal to 883 mm^3. In this case, provided that the fuel is injected at room temperature ($T_d = 300$ K) into air at temperature of 880 K and pressure of 3 MPa, and when all the fuel has evaporated without combusting, the fuel vapour/air mixture is expected to become close to stoichiometric. More precisely, the equivalence ratio for n-dodecane in these conditions was calculated as 0.98, while for diesel fuel it was calculated as 1.01. This calculation took into account the relevant physical properties including temperature dependence of the liquid fuel density. The liquid fuel physical properties were calculated based on average droplet temperature of $\overline{T}_d$. Their initial velocities were taken in the range from 0 to 100 $m \cdot s^{-1}$. Droplet initial diameters were taken equal to 5, 20 and 50 μm. The initial gas pressure and temperature were taken in the ranges from 1 to 5.5 MPa and from 700 to 1200 K, respectively. In this case the equivalence ratios of the mixture of evaporated fuel and air are expected to change accordingly, and are shown in Figs. 7(a), (b). External temperatures, responsible for radiative heating of droplets, were taken in the range from 880 to 2500 K. The flammability equivalence ratio of fuel was taken in the range from 0.5 to 5 [41]. The autoignition process was modelled based on the version of the Shell model described in [40, 41] with the constant A_{f4} in the range between 3×10^6 and

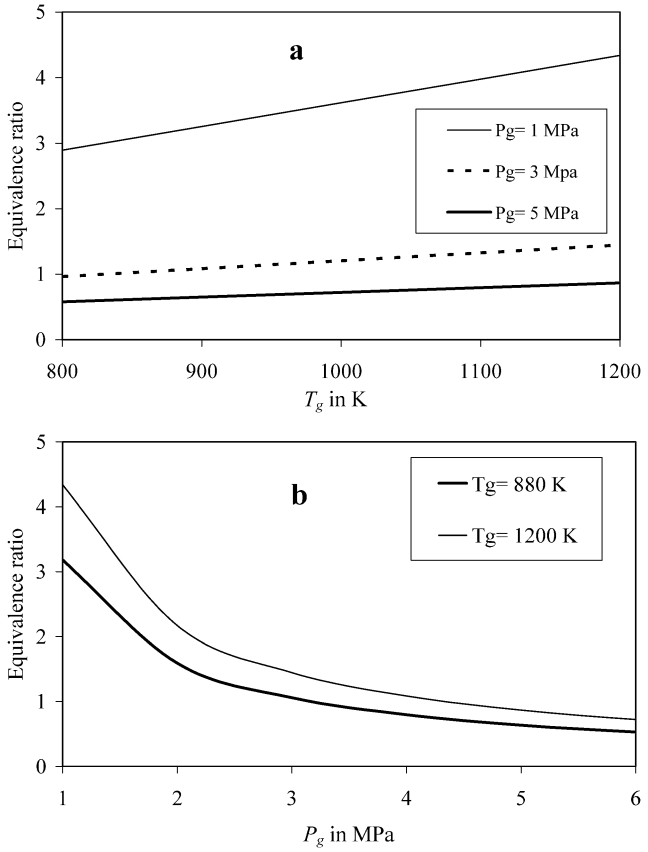

Fig. 7. The values of the equivalence ratio versus gas temperature for various gas pressures (a), and the values of the equivalence ratio versus gas pressure for various gas temperatures (b). 1 mm^3 of liquid *n*-dodecane was injected into 883 mm^3.

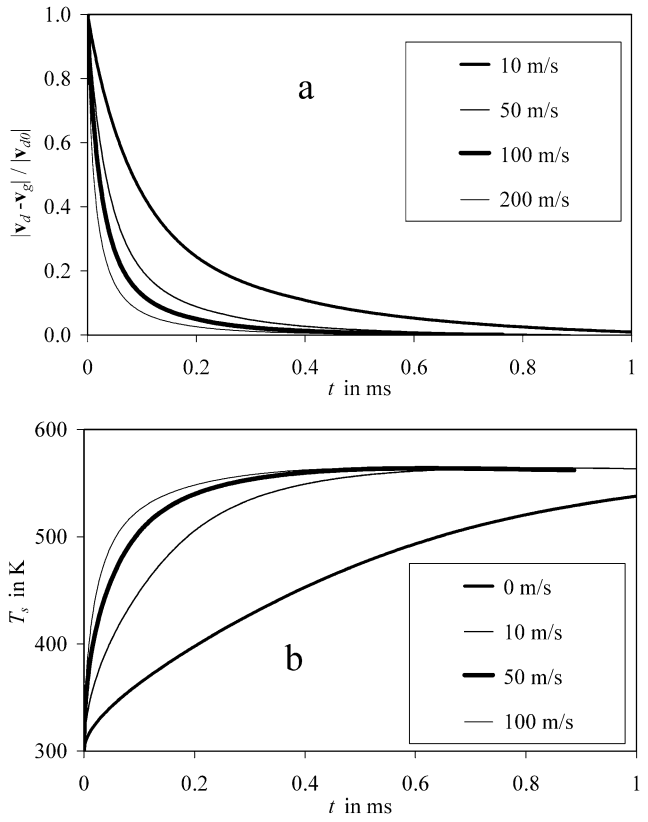

Fig. 8. Plots of $|\mathbf{v}_d - \mathbf{v}_g|/|\mathbf{v}_{d0}|$ ($\mathbf{v}_{d0}$ is the initial droplet velocity) versus time for $|\mathbf{v}_{d0}| = 10$, 50, 100 and 200 $m{\cdot}s^{-1}$ (a), and plots of the droplet surface temperature T_s versus time for $|\mathbf{v}_{d0}| = 0$, 10, 50 and 100 $m{\cdot}s^{-1}$ (b). In all cases $\mathbf{v}_{g0} = 0$. The initial gas temperature is equal to 880 K, initial gas pressure is equal to 3 MPa, and *n*-dodecane droplet with initial temperature and radius equal to 300 K and 10 μm, respectively are taken. The ETC model is used and the effect of thermal radiation is ignored.

6×10^6. The autoignition process was assumed to be completed when the fuel vapour/air temperature reached 1100 K.

To illustrate the effect of initial droplet velocities on the time evolution of the relative droplet velocities and their surface temperatures we consider the case when the initial gas temperature is equal to 880 K, initial gas pressure equal to 3 MPa, and *n*-dodecane droplet initial temperature and radius equal to 300 K and 10 μm, respectively. The ETC model is used and the effect of thermal radiation is ignored (this effect is illustrated in Fig. 3). In Fig. 8(a) the plots of relative droplet velocities $|\mathbf{v}_d - \mathbf{v}_g|/|\mathbf{v}_{d0}|$ ($\mathbf{v}_{d0}$ is the initial droplet velocity) versus time for $|\mathbf{v}_{d0}| = 10$, 50, 100 and 200 $m{\cdot}s^{-1}$, are presented. The initial gas velocity is assumed equal to zero. As follows from this figure, the rate of decrease of the relative velocity increases with increasing $|\mathbf{v}_{d0}|$. As a result, regardless of the values of the initial velocities, the velocities of all droplets approach to the gas velocity. The plots of the droplet surface temperature T_s versus time for $|\mathbf{v}_{d0}| = 0$, 10, 50 and 100 $m{\cdot}s^{-1}$ are presented in Fig. 8(b). As follows from this figure, the rate of increase of this temperature increases with increasing droplet initial velocity. This would be expected as the convective heat transfer coefficient increases with increasing Re and the initial droplet velocities (see Eq. (1)). Also, as expected in the absence of thermal radiation, in all cases the droplet surface temperature asymptotically approach the wet bulb temperature. All the above mentioned properties of the curves shown in Fig. 8 can be observed for the initial values of droplet diameters equal to 5 and 50 μm and other values of the initial gas temperature and pressure.

The following analysis is focused on the calculation of the droplet evaporation time. We assume that gas temperature and pressure are equal to 880 K and 3 MPa, respectively, and consider *n*-dodecane droplets with diameters 5, 20, and 50 μm, moving with initial velocities 0 (stationary droplets), 10, 50, and 100 $m{\cdot}s^{-1}$. These are typical parameter values for diesel engines [41]. Also, we consider the values of external temperatures in the range from 880 K (gas temperature) to 2500 K (maximal temperature of remote flames in the engine [41]). It was shown that the effect of temperature gradient inside droplets and recirculation in them generally leads to a slight increase in evaporation time: less than 1.7, 1.9 and 3% for droplet initial diameters 5, 20, and 50 μm, respectively. A similar analysis of these droplets evaporation without the contribution of radiation, but for initial gas temperatures in the range (700–1200 K) has shown that the effect of temperature gradient inside these droplets and re-

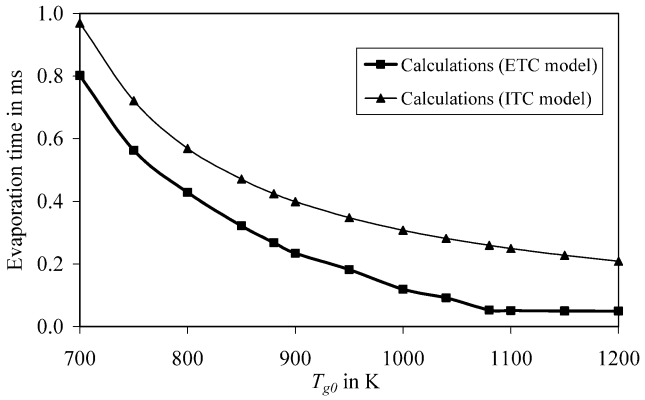

Fig. 9. The values of the evaporation time versus initial gas temperature calculated based on the ITC and the ETC models implemented into the algorithm described in Section 2. Bag and stripping droplet break-ups were taken into account. The initial droplet diameter and velocity are taken equal to 50 μm and 50 m·s^{-1}, respectively. Symbols indicate the values of gas temperature for which the evaporation times were calculated.

circulation in them generally leads to the corresponding increases of evaporation time by less than 2.5, 3.5 and 5%, respectively. A similar analysis but for fixed gas temperature without radiation but for initial pressures in the range (1–5.5) MPa led to the corresponding increases of evaporation time less than 1.9, 2.1 and 4%. Hence, this effect of the temperature gradient inside droplets on their evaporation time can certainly be ignored in most applications. Analysis of diesel fuel droplets led to an essentially similar conclusion.

Fig. 9 illustrates the effect of a ETC model on droplet evaporation time at various initial gas temperatures in the presence of break-up. The initial droplet diameter and velocity are assumed equal to 50 μm and 50 m·s^{-1}, respectively. If the conditions for both bag and stripping break-up are satisfied simultaneously, then if $t_b < t_s$ then it is assumed that only bag break-up takes place and vice versa. Symbols in the figure indicate the values of gas temperature for which calculations of the evaporation time were performed.

As one can see from Fig. 9, in the presence of break-up the ETC model predicts noticeably shorter evaporation times when compared with the ITC model, especially at high initial gas temperatures. This result can be related to rather strong dependence of the surface tension coefficient on droplet surface temperature T_s, which is translated into the corresponding dependence of $R_{db(s)}$ and t_b on T_s. Remembering Eq. (13), ignoring the temperature dependence of ρ_d and assuming that v_g and v_d are constant, we can find the following expressions for the ratios:

$$\widetilde{R}_{db} \equiv \frac{R_{db}(T_s)}{R_{db}(T_s = 300\ \mathrm{K})} = \frac{\sigma_s(T_s)}{\sigma_s(T_s = 300\ \mathrm{K})} \times \frac{T_g + 2T_s}{T_g + 600}$$

$$\widetilde{R}_{ds} \equiv \frac{R_{ds}(T_s)}{R_{ds}(T_s = 300\ \mathrm{K})} = \widetilde{R}_{db}^2$$

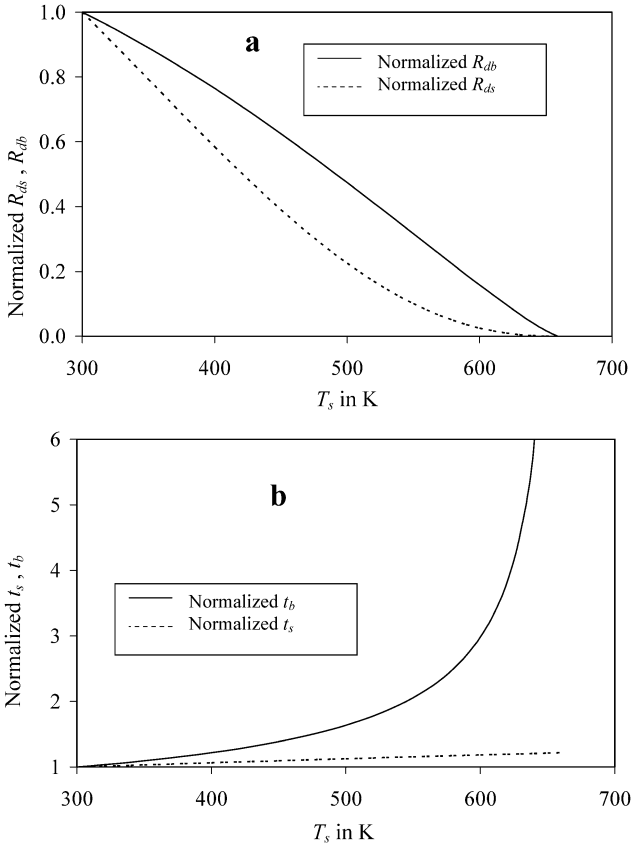

Fig. 10. Values of $\widetilde{R}_{db} \equiv R_{db}(T_s)/R_{db}(T_s = 300\ \mathrm{K})$, $\widetilde{R}_{ds} \equiv R_{ds}(T_s)/R_{ds}(T_s = 300\ \mathrm{K})$ (a), $\tilde{t}_b \equiv t_b(T_s)/t_b(T_s = 300\ \mathrm{K})$, $\tilde{t}_s \equiv t_s(T_s)/t_s(T_s = 300\ \mathrm{K})$ (b) versus droplet surface temperature.

$$\tilde{t}_b \equiv \frac{t_b(T_s)}{t_b(T_s = 300\ \mathrm{K})} = \sqrt{\frac{\sigma_s(T_s)}{\sigma_s(T_s = 300\ \mathrm{K})}}$$

$$\tilde{t}_s \equiv \frac{t_s(T_s)}{t_s(T_s = 300\ \mathrm{K})} = \sqrt{\frac{T_g + 2T_s}{T_g + 600}}$$

The plots of $\widetilde{R}_{db}$, $\widetilde{R}_{ds}$, $\tilde{t}_b$ and $\tilde{t}_s$ versus T_s for n-dodecane are shown in Figs. 10(a), (b). As can be seen from Fig. 10(a), both $\widetilde{R}_{db}$ and $\widetilde{R}_{ds}$ decrease rather rapidly with increasing T_s, mainly due to the fact that surface tension decreases with increasing T_s. Since the ETC model predicts more rapid initial increase of T_s compared with the ITC model, one can expect that the break-up process is predicted by the ETC model for a wider range of droplet radii, compared with the prediction of the ITC model. Hence the evaporation of droplets, as predicted by the ETC model, is expected to be more rapid when compared with the predictions of the ITC model. This is consistent with the results shown in Fig. 9.

As follows from Fig. 10(b), the increase of $\tilde{t}_s$ with increasing T_s is rather weak and can be ignored in most practical application. The increase of $\tilde{t}_b$ with increasing T_s is also weak at low T_s ($T_s < 400$ K), but $\tilde{t}_b$ increases rather rapidly with T_s at $T_s > 400$ K. This increase of $\tilde{t}_b$ alone would lead to a slow down of the bag break-up as predicted by the ETC model. In the case shown in Fig. 9, the intensification of the

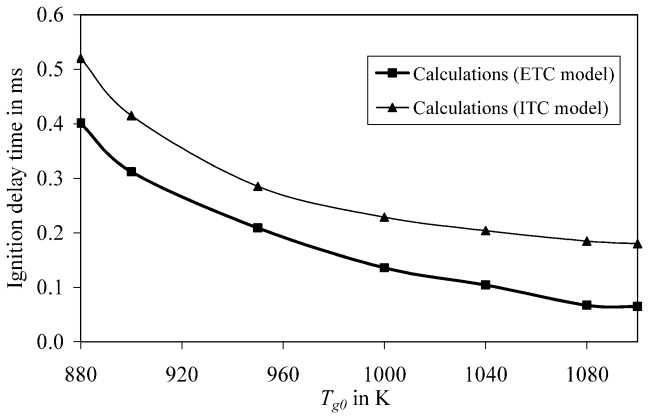

Fig. 11. The plots of the total ignition delay versus T_s in the presence of the break-up for the same droplets as used in Fig. 8, calculated based on the ITC and the ETC models implemented into the algorithm described in Section 2. Symbols indicate the values of gas temperature for which the ignition delay times were calculated.

break-up process due to the reduction of $\widetilde{R}_{db}$ and $\widetilde{R}_{ds}$ seems to dominate the slow down due to increase of $\tilde{t}_b$ and $\tilde{t}_s$. Similar results were obtained for diesel fuel.

The plots of the total ignition delay versus T_s in the presence of break-up for the same droplets as used in Fig. 9, are shown in Fig. 11. The Shell model with $A_{f4} = 3 \times 10^6$ was used. As can be seen from this figure, the ignition delay decreases with increasing T_g. The effect of temperature gradient inside droplets and recirculation in them on the total ignition delay is consistent with the predictions of Fig. 6. As in Fig. 9, symbols indicate the values of initial gas temperature for which the calculations were performed.

Strong influence of the temperature gradient inside droplets on droplet break-up, evaporation and the ignition of evaporated fuel/air mixture, allows us to recommend that this effect is taken into account in computational fluid dynamics codes designed to model fluid dynamics, heat transfer and combustion processes in internal combustion engines. So far this effect has been almost universally ignored, with the only exception of this, to the best of our knowledge, being paper [22].

It should be mentioned that the zero-dimensional analysis presented in this paper has well known limitations in predicting the actually observed total ignition delay of fuel droplets. At least a one-dimensional analysis of the gas phase would be required to describe adequately the fuel vapour diffusion around droplets. This would ultimately control the ignition process of the fuel vapour/air mixture (see [47] and [50–54]). Nevertheless we see the importance of the current work in the following directions. Firstly, it can be considered as the first step and motivation to continue the started work of introducing the temperature gradient in modelling of droplet evaporation and break-up for appropriate conditions. Secondly the model described in the paper is presented in a form suitable for implementation into multidimensional CFD codes, where the individual computational cells are assumed to be free from spatial inhomogeneities.

5. Conclusion

A zero-dimensional code taking into account the temperature gradient inside droplets, the coupling between liquid and gas phases and describing the autoignition process based on the Shell autoignition model has been developed. This code was used to study the effects of temperature gradient inside fuel droplets on droplet evaporation, break-up and the ignition of fuel vapour/air mixture. The predictions of the code are validated against experimental data published by Belardini et al. [45], Nomura et al. [46], and Tanabe et al. [47]. In the absence of break-up, the influence of temperature gradient on droplet evaporation in realistic diesel engine conditions is generally small (1–3%). In the presence of the break-up process, however, the temperature gradient inside droplets can lead to a significant decrease in the evaporation time under the same conditions. This is attributed to the fact that the effect of the temperature gradient inside droplets leads to a substantial increase in droplet surface temperature at the initial stages of its heating. This increase, in turn, leads to a decrease in droplet surface tension and a decrease in the threshold radii at which break-up occurs, assuming that bag and stripping break-ups are the dominant mechanisms of droplet break-up. Even in the absence of break-up, the effect of temperature gradient inside droplets leads to a noticeable (up to about 20%) decrease of the total ignition delay time (comprising the physical and chemical ignition delays). In the presence of break-up, this effect is enhanced substantially, leading to more than halving of the total ignition delay. This reduction of the total ignition delay time is understood to be due to the combined effect of the influence of increased droplet surface temperature on the chemical ignition delay, and the influence of this temperature on droplet evaporation (in the presence of break-up processes). It is recommended that the effects of temperature gradient inside droplets are taken into account in computational fluid dynamics codes describing droplet break-up and evaporation processes, and the ignition of the evaporated fuel/air mixture.

Acknowledgement

The authors are grateful to the EPSRC (grant GR/R82920/01) for the financial support of this project.

Appendix A

A.1. Physical properties of tetradecane

Using data presented in [55], the latent heat of evaporation in $J \cdot kg^{-1}$ was approximated as:

$$L = 4.7999679442 \times 10^5 - 447.99679239T + 1.0772809826T^2 - 8.4415064357 \times 10^{-3}T^3 + 2.907585478 \times 10^{-5}T^4 - 4.3509615486 \times 10^{-8}T^5 + 2.1527777826 \times 10^{-11}T^6$$

when $T < T_{cr} = 693$ K (critical temperature) and zero otherwise [56].

Using data presented in [55], the specific heat capacity of liquid in $J{\cdot}kg^{-1}{\cdot}K^{-1}$ is approximated as:

$$c_l = 1453.5010887 \times \exp(0.0014122933017T)$$

The specific heat capacity of vapour at constant pressure is approximated as [56]:

$$c_{pF} = -1.7787319 + 6.4564177T - 3.2454867 \times 10^{-3}T^2 + 4.5752023 \times 10^{-7}T^3 + 8.510382 \times 10^{-11}T^4$$

The saturated vapour pressure is assumed to be equal to

$$p_s = 10^5 \times 10^{4.1379-1740.88/(T-105.43)}\ N{\cdot}m^{-2}$$

when $T < T_{cr}$, and zero otherwise [56]. Using data presented in [55], the density of liquid is approximated as

$$\rho_l = 915.017 - 0.366493T - 4.68132 \times 10^{-4}T^2$$

and the thermal conductivity of liquid in $W{\cdot}m^{-1}{\cdot}K^{-1}$ is approximated as

$$k_l = 0.16243019148 + 1.1551271437 \times 10^{-4}T - 7.6492882118 \times 10^{-7}T^2 + 5.9731934732 \times 10^{-10}T^3$$

when $T < T_{cr}$, and zero otherwise.

A.2. Physical properties of n-heptane

Latent heat of evaporation in $J{\cdot}kg^{-1}$ is approximated as [57]:

$$L = 317.8 \times 10^3\left(\frac{T_{cr}-T}{T_{cr}-T_b}\right)^{0.38}$$

where $T_{cr} = 540.17$ K and $T_b = 371.4$ K [56], when $T < T_{cr}$, and zero otherwise. Using data presented in [55], the specific heat capacity of liquid in $J{\cdot}kg^{-1}{\cdot}K^{-1}$ is approximated as:

$$c_l = 13058.45044066 - 126.5095282565T + 0.5279613848638T^2 - 0.0009457386295687T^3 + 6.369853422618 \times 10^{-7}T^4$$

The specific heat capacity of vapour at constant pressure is approximated as [56]:

$$c_{pF} = 799.3401062 + 0.3448263942T + 0.01285548641T^2 - 1664.890863 \times 10^{-8}T^3 + 644.6826474 \times 10^{-11}T^4$$

The saturated vapour pressure is assumed to be equal to

$$p_s = 10^5 \times 10^{4.02677-1258.34/(T-53.85)}\ N{\cdot}m^{-2}$$

when $T < T_{cr}$, and zero otherwise [56]. Using data presented in [55], the density of liquid is approximated as

$$\rho_l = -941.03 + 19.96181T - 0.08612051T^2 + 1.579494 \times 10^{-4}T^3 - 1.089345 \times 10^{-7}T^4$$

when $T \leqslant 538$ K, and

$$\rho_l = 4.195281 \times 10^7 - 2.360524 \times 10^5T + 442.7316T^2 - 0.2767921T^3$$

when $T > 538$ K. Using data presented in [55], the thermal conductivity of liquid in $W{\cdot}m^{-1}{\cdot}K^{-1}$ is approximated as:

$$k_l = 0.25844890110 - 4.5549450549 \times 10^{-4}T$$

when $T < T_{cr}$, and zero otherwise.

A.3. Physical properties of n-dodecane

Latent heat of evaporation in $J{\cdot}kg^{-1}$ [60]:

$$L = 329037.62 + 1883.02T - 10.99644T^2 + 0.021056T^3 - 1.44737 \times 10^{-5}T^4$$

when $T < T_{cr} = 659$ K (critical temperature) [56], and zero otherwise.

Using data presented in [55], the specific heat capacity of liquid in $J{\cdot}kg^{-1}{\cdot}K^{-1}$ is approximated as: $c_l = 803.42 + 5.076T - 0.00221T^2 + 1.673 \times 10^{-6}T^3$. The specific heat capacity of vapour at constant pressure is approximated as [59]:

$$c_{pF} = 380.63 + 4.1372T + 2.004 \times 10^{-4}T^2 - 1.8009 \times 10^{-6}T^3 + 7.7875 \times 10^{-10}T^4 - 1.0152 \times 10^{-13}T^5$$

The saturated vapour pressure is assumed to be equal to

$$p_s = 6894.757 \times \exp\left[12.12767 - 3743.84/(T - 93.022)\right]$$

when $T < T_{cr}$, and zero otherwise. The density of liquid is approximated as [58]

$$\rho_l = 1104.98 - 1.9277T + 0.003411T^2 - 3.2851 \times 10^{-6}T^3$$

The thermal conductivity of liquid n-dodecane and liquid diesel fuel in $W{\cdot}m^{-1}{\cdot}K^{-1}$ was used in the table form (see [56, Table 1]).

The surface tension is approximated as [59]:

$$\sigma_s = 0.0528\left(1 - \frac{T}{T_{cr}}\right)^{0.121}$$

A.4. Physical properties of diesel fuel

In this section a compilation of physical properties of a 'typical' diesel fuel is given. These are expected to differ slightly from any particular diesel fuel.

Table 1

T [K]	k_l [W·m^{-1}·K^{-1}]	
	diesel fuel	n-dodecane
250	0.156	0.150
260	0.153	0.148
270	0.151	0.146
280	0.149	0.143
290	0.147	0.141
300	0.145	0.139
310	0.143	0.136
320	0.141	0.134
330	0.139	0.132
340	0.137	0.130
350	0.135	0.128
360	0.133	0.126
370	0.131	0.123
380	0.129	0.121
390	0.127	0.119
400	0.125	0.117
410	0.123	0.115
420	0.121	0.112
430	0.119	0.110
440	0.117	0.108
450	0.115	0.106
460	0.113	0.103
470	0.111	0.101
480	0.109	0.098
490	0.107	0.096
500	0.104	0.093
510	0.102	0.091
520	0.100	0.088
530	0.098	0.086
540	0.096	0.083
550	0.094	0.080
560	0.091	0.077
570	0.089	0.073
580	0.086	0.070
590	0.084	0.066
600	0.081	0.062
610	0.078	0.058
620	0.076	0.053
630	0.073	0.047
640	0.069	0.040
650	0.066	0.030
660	0.062	0
670	0.059	0
680	0.054	0
690	0.049	0
700	0.043	0
710	0.036	0
720	0.025	0
730	0	0

Latent heat of evaporation in J·kg^{-1} [57]:

$$L = 254 \times 10^3 \left(\frac{T_{\rm cr} - T}{T_{\rm cr} - T_b} \right)^{0.38}$$

where $T_{\rm cr} = 725.9$ K and $T_b = 536.4$ K, when $T < T_{\rm cr}$, and zero otherwise.

The specific heat capacity of liquid in J·kg^{-1}·K^{-1} is approximated as [59]: $c_l = 264 + 6.33T - 0.00296T^2$. The specific heat capacity of vapour at constant pressure is approximated as equal to that of n-dodecane [59]. The saturated vapour pressure is assumed to be equal to [57]:

$$p_s = \begin{cases} 1000 \times \exp\left[8.5872101 - 2591.5232/(T-43)\right] \\ \quad \text{when } T < 380 \text{ K} \\ 1000 \times \exp\left[14.060729 - 4436.099/(T-43)\right] \\ \quad \text{when } 380 \leqslant T < 500 \text{ K} \\ 1000 \times \exp\left[12.93692 - 3922.5184/(T-43)\right] \\ \quad \text{when } 500 \leqslant T < 620 \text{ K} \\ 1000 \times \exp\left[16.209535 - 5810.817/(T-43)\right] \\ \quad \text{when } 620 \leqslant T < T_{\rm cr} \text{ K} \\ 0 \quad \text{when } T \geqslant T_{\rm cr} \text{ K} \end{cases}$$

The density of liquid is approximated as [58]: $\rho_l = 840/[1 + 0.00067(T - 288)]$. The thermal conductivity of liquid in W·m^{-1}·K^{-1} is presented in Table 1 [56]

The surface tension is approximated as [59]:

$$\sigma_s = 0.059 \left(1 - \frac{T}{T_{\rm cr}} \right)^{0.121}$$

References

[1] R. Clift, J.R. Grace, M.E. Weber, Bubbles, Drops and Particles, Academic Press, New York, 1978.

[2] G.M. Faeth, Evaporation and combustion of sprays, Progr. Energy Combust. Sci. 9 (1983) 1–76.

[3] K.-K. Kuo, Principles of Combustion, Wiley, New York, 1996.

[4] A.H. Lefebvre, Atomization and Sprays, Taylor & Francis, Bristol, PA, 1989.

[5] B. Abramzon, W.A. Sirignano, Droplet vaporization model for spray combustion calculations, Internat. J. Heat Mass Transfer 32 (1989) 1605–1618.

[6] S.K. Aggarwal, A review of spray ignition phenomena: Present status and future research, Progr. Energy Combust. Sci. 24 (1998) 565–600.

[7] J.F. Griffiths, J.A. Barnard, Flame and Combustion, Blackie Academic & Professional, 1995.

[8] G.L. Borman, K.W. Ragland, Combustion Engineering, McGraw-Hill, New York, 1998.

[9] W.A. Sirignano, Fluid Dynamics and Transport of Droplets and Sprays, Cambridge University Press, Cambridge, 1999.

[10] E.E. Michaelides, Hydrodynamic force and heat/mass transfer from particles, bubbles, and drops—the Freeman scholar lecture, ASME J. Fluid Engrg. 125 (2003) 209–238.

[11] L.A. Dombrovsky, S.S. Sazhin, E.M. Sazhina, G. Feng, M.R. Heikal, M.E.A. Bardsley, S.V. Mikhalovsky, Heating and evaporation of semi-transparent diesel fuel droplets in the presence of thermal radiation, Fuel 80 (2001) 1535–1544.

[12] L.A. Dombrovsky, S.S. Sazhin, A parabolic temperature profile model for heating of droplets, ASME J. Heat Transfer 125 (2003) 535–537.

[13] L.A. Dombrovsky, S.S. Sazhin, A simplified non-isothermal model for droplet heating and evaporation, Internat. Commun. Heat Mass Transfer 30 (6) (2003) 787–796.

[14] L.A. Dombrovsky, S.S. Sazhin, Absorption of thermal radiation in a semi-transparent spherical droplet: a simplified model, Internat. J. Heat Fluid Flow 24 (6) (2003) 919–927.

[15] S.S. Sazhin, W.A. Abdelghaffar, E.M. Sazhina, S.V. Mikhalovsky, S.T. Meikle, C. Bai, Radiative heating of semi-transparent diesel fuel droplets, ASME J. Heat Transfer 126 (2004) 105–109;
S.S. Sazhin, W.A. Abdelghaffar, E.M. Sazhina, S.V. Mikhalovsky, S.T. Meikle, C. Bai, ASME J. Heat Transfer 126 (2004) 490–491, Erratum.

[16] A.P. Kryukov, V.Yu. Levashov, S.S. Sazhin, Evaporation of diesel fuel droplets: Kinetic versus hydrodynamic models, Internat. J. Heat Mass Transfer 47 (12–13) (2004) 2541–2549.

[17] L.A. Dombrovsky, S.S. Sazhin, Absorption of external thermal radiation in asymmetrically illuminated droplets, J. Quantitative Spectroscopy Radiation Transfer 87 (2004) 119–135.

[18] L.A. Dombrovsky, Absorption of thermal radiation in large semi-transparent particles at arbitrary illumination of a polydisperse system, Internat. J. Heat Mass Transfer 47 (2004) 5511–5522.
[19] S.S. Sazhin, P.A. Krutitskii, W.A. Abdelghaffar, S.V. Mikhalovsky, S.T. Meikle, M.R. Heikal, Transient heating of diesel fuel droplets, Internat. J. Heat Mass Transfer 47 (2004) 3327–3340.
[20] S.S. Sazhin, P.A. Krutitskii, W.A. Abdelghaffar, E.M. Sazhina, M.R. Heikal, Transient heating of droplets, in: G.P. Celata, et al. (Eds.), Proceedings of '3rd International Symposium on Two-Phase Flow Modelling and Experimentation', Pisa 22–24 September 2004, Begell House, 2004, paper bja01 (CD-ROM).
[21] B. Abramzon, S.S. Sazhin, Droplet vaporization model in the presence of thermal radiation, Internat. J. Heat Mass Transfer 48 (2005) 1868–1873.
[22] C. Bertoli, M. Migliaccio, A finite conductivity model for diesel spray evaporation computations, Internat. J. Heat Fluid Flow 20 (1999) 552–561.
[23] S.S. Sazhin, C. Crua, D. Kennaird, M.R. Heikal, The initial stage of fuel spray penetration, Fuel 82 (2003) 875–885.
[24] S. Hohmann, U. Renz, Numerical simulation of fuel sprays at high ambient pressure: The influence of real gas effects and gas solubility on droplet vaporisation, Internat. J. Heat Mass Transfer 46 (2003) 3017–3028.
[25] J. Bellan, Supercritical (and subcritical) fluid behavior and modelling: Drops, steams, shear and mixing layers, jets and sprays, Progr. Energy Combust. Sci. 26 (2000) 329–366.
[26] S.D. Givler, J. Abraham, Supercritical droplet vaporization and combustion studies, Progr. Energy Combust. Sci. 22 (1996) 1–28.
[27] E. Loth, Numerical approaches for motion of dispersed particles, droplets and bubbles, Progr. Energy Combust. Sci. 26 (2000) 161–223.
[28] M. Orme, Experiments on droplet collisions, bounce, coalescence and disruption, Progr. Energy Combust. Sci. 23 (1997) 65–79.
[29] R.B. Bird, W.E. Stewart, E.N. Lightfoot, Transport Phenomena, Wiley, New York, 2002.
[30] G.F. Yao, S.I. Abdel-Khalik, S.M. Ghiaasiaan, An investigation of simple evaporation models used in spray simulations, ASME J. Heat Transfer 125 (1997) 179–182.
[31] A.B. Liu, R.D. Reitz, Mechanisms of air-assited liquid atomization, Atomization Sprays 3 (1993) 55–75.
[32] F.X. Tanner, Development and validation of a cascade atomization and droplet break-up model for high-velocity dense sprays, Atomization Sprays 14 (2004) 211–242.
[33] L. von Schiller, A. Naumann, Über die grundlegenden Berechnungen bei der Schwerkraftaufbereitung, Z. Vereines Deutscher Ingenieure 44 (1933) 318–320.
[34] Z.-G. Feng, E.E. Michaelides, Heat and mass transfer coefficients of viscous spheres, Internat. J. Heat Mass Transfer 44 (2001) 4445–4454.
[35] R.L. Panton, Incompressible Flow, Wiley, New York, 1996.
[36] R.D. Reitz, R. Diwakar, Effect of drop breakup on fuel sprays, SAE Report 860469, 1986.
[37] R.D. Reitz, R. Diwakar, Structure of high-pressure fuel sprays, SAE Report 870598, 1987.
[38] S.S. Sazhin, P. Wild, C. Leys, D. Toebaert, E.M. Sazhina, The three temperature model for the fast-axial-flow CO_2 laser, J. Phys. D: Appl. Phys. 26 (1993) 1872–1883.
[39] M.R. Halstead, L.J. Kirsch, C.P. Quinn, The autoignition of hydrocarbon fuels at high temperatures and pressures—fitting of a mathematical model, Combust. Flame 30 (1977) 45–60.
[40] E.M. Sazhina, S.S. Sazhin, M.R. Heikal, C. Marooney, The Shell autoignition model: application to gasoline and Diesel fuels, Fuel 78 (4) (1999) 389–401.
[41] E.M. Sazhina, S.S. Sazhin, M.R. Heikal, V.I. Babushok, R. Johns, A detailed modelling of the spray ignition process in Diesel engines, Combust. Sci. Technol. 160 (2000) 317–344.
[42] P. Laveille, F. Lemoine, M. Labouché, Measurement of the temperature distribution over a combusting droplet in monodisperse stream using two colors laser-induced fluorescence, in: Taine J. (Ed.), Proceedings of the 12th International Heat Transfer Conference, vol. 2, Elsevier, Paris, 2002, p. 917 (available on CD).
[43] G. Castanet, P. Laveille, F. Lemoine, M. Labouché, A. Atthasit, Y. Biscos, G. Lavergne, Energetic budget on an evaporating monodisperse droplet stream using combined optical methods. Evaluation of the convective heat transfer, Internat. J. Heat Mass Transfer 45 (2002) 5053–5067.
[44] G. Castanet, P. Laveille, M. Labouché, F. Lemoine, Measurements of the temperature distribution within monodisperse combusting droplets in linear streams using two-color laser-induced fluorescence, Experiments Fluids 35 (2003) 563–571.
[45] P. Belardini, C. Bertoli, M. Lazzaro, P. Massoli, Single droplet evaporation rate: Experimental and numerical investigations, in: Proceedings of the Second International Conference on Fluid-Mechanics, Combustion, Emissions and Reliability in Reciprocating Engines Capri, Italy, 1992, pp. 265–270.
[46] H. Nomura, Y. Ujiie, H.J. Rath, J. Sato, M. Kono, Experimental study on high-pressure droplet evaporation using microgravity conditions, in: 26th Symposium (International) on Combustion, The Combustion Institute, 1996, pp. 1267–1273.
[47] M. Tanabe, M. Kono, J. Sato, J. Koenig, C. Eigenbrod, F. Dinkelacker, H.J. Rath, Two stage ignition of *n*-heptane isolated droplets, Combust. Sci. Technol. 108 (1995) 103–119.
[48] O.M. Todes, Quasi-stationary regimes of mass and heat transfer between a spherical body and ambient medium, in: V.A. Fedoseev (Ed.), Problems of Evaporation, Combustion and Gas Dynamics of Disperse Systems. Proceedings of the Sixths Conference on Evaporation, Combustion and Gas Dynamics of Disperse Systems, October 1966, Odessa University Publishing House, Odessa, 1968, pp. 151–159 (in Russian).
[49] S.S. Sazhin, V. Goldshtein, M.R. Heikal, A transient formulation of Newton's cooling law for spherical bodies, ASME J. Heat Transfer 123 (1) (2001) 63–64.
[50] S. Schnaubelt, O. Moriue, T. Coordes, C. Eigenbrod, H.J. Rath, Detailed numerical simulations of the multiscale self-ignition process of *n*-heptane isolated droplets and their verification by comparison with microgravity experiments, Proc. Combust. Instit. 28 (2000) 953–960.
[51] S.M. Frolov, V.Ya. Basevich, A.A. Belyaev, V.S. Posvyanskii, V.A. Smetanyuk, Detailed modeling of drop evaporation and combustion, in: G.D. Roy, S.M. Frolov, A.M. Starik (Eds.), Combustion and Atmospheric Pollution, Torus Press, Moscow, 2003, pp. 207–213.
[52] S.M. Frolov, A.A. Scripnik, R.Z. Kavtaradze, Modelling of diesel spray ignition, in: G.D. Roy, S.M. Frolov, A.M. Starik (Eds.), Combustion and Atmospheric Pollution, Torus Press, Moscow, 2003, pp. 220–227.
[53] O. Moriue, S. Schnaubelt, C. Eigenbrod, H.J. Rath, Numerical simulation of the ignition of a single fuel droplet in an air with finite volume, in: Proceedings of 9th International Conference on Liquid Atomization and Spray Systems, Sorrento, Italy, paper 0701 on a CD, 2003.
[54] G.L. Hubbard, V.E. Denny, A.F. Mills, Droplet evaporation: effects of transient and variable properties, Internat. J. Heat Mass Transfer 18 (1975) 1003–1008.
[55] J.B. Maxwell, Data Book on Hydrocarbons: Application to Process Engineering, van Nostrand, New York, 1950.
[56] B.E. Poling, J.M. Prausnitz, J. O'Connell, The Properties of Gases and Liquids, McGraw-Hill, New York, 2000.
[57] J.S. Chin, A.H. Lefebvre, The role of the heat-up period in fuel drop evaporation, Internat. J. Turbo Jet Engines 2 (1985) 315–325.
[58] Handbook of Aviation Fuel Properties, SAE CRC Technical Report No. 530, 1984.
[59] R.P. Durret., D.C. Oren, C.R. Ferguson, A Multidimensional Data Set for Diesel Combustion Model Validation: I. Initial Conditions, Pressure History and Spray Shapes, SAE Technical Report 872087, 1987.
[60] G.L. Borman, J.H. Johnson, Unsteady Vaporization Histories and Trajectories of Fuel Drops Injected Into Swirling Air, SAE Technical Report 620271, 1962.